JOURNAL OF MATERIALS SCIENCE 19 (1984) 2815–2836

Strengthening mechanisms in Elgiloy

M. ASSEFPOUR-DEZFULY, W. BONFIELD
Department of Materials, Queen Mary College, London, E1 4NS, UK

The effects of cold-working and age-hardening on the microstructure of Elgiloy (composition in wt %, 40 Co, 20 Cr, 15 Ni, 7 Mo, 2 Mn, 0.1 C, balance Fe) have been established. 36% and 72% cold reduction of the solution treated (ST) alloy (f c c) produced a network of thin f c c deformation twins and h c p ϵ-martensite platelets. The subsequent age-hardening of the cold-worked strip noted at 500° C was attributed to the formation of additional ϵ-phase (via the $\alpha_{fcc} \rightleftharpoons \epsilon_{hcp}$ transformation), whereas the ST condition did not harden significantly at this temperature. In contrast, ageing the ST condition at 800° C for periods > 1000 h caused an increase in hardness due to the formation of a coarse Mo–Co–Cr intermetallic compound together with a smaller amount of $M_{23}C_6$ carbide, while age softening of the cold-worked strip occurred at this temperature as a result of recovery and dissolution of the deformation induced ϵ-phase.

1. Introduction

Elgiloy is a cobalt-based alloy of composition in w %, 40 Co, 20 Cr, 15 Ni, 7 Mo, 2 Mn, 0.1 C, balance Fe (15.9), which initially found application as mainsprings in watches. but has also proved suitable as a spring element in inertial navigation instruments, and has generally been used in the cold-worked condition. The available literature on the structure–mechanical properties relationship and age-hardening behaviour in this alloy is limited and contradictory. For example Trickey's [1] conclusion that Elgiloy precipitation hardens in the same manner as copper–beryllium is in contrast to the suggestion [2] that Elgiloy derives its maximum properties from a combination of cold-work and heat treatment and is not a true precipitation hardening alloy. Alternatively, Henmi *et al.* [3] attributed age hardening of cold-worked Elgiloy to precipitation of "fine" α-cobalt particles (h c p phase of cobalt), while Legendre and Wache [4] proposed a disorder–order transformation.

The aim of this investigation was to attempt to clarify the mechanisms of deformation induced hardening and age-hardening in Elgiloy. The alloy was studied in the solution treated (ST), 36% cold-worked (36% CW) and 72% cold-worked (72% CW) conditions and the subsequent age-hardening behaviour in the temperature range 400 to 900° C was established.

2. Experimental details

Elgiloy was supplied by the Royal Aircraft Establishment in the form of strips which had been cold-worked by rolling to 36% (36% CW) and 72% (72% CW) reductions. The compositions of the strip as specified by the manufacturer and as determined by an independent chemical analysis are given in Table I. The solution treated (ST) condition was prepared by heat treating the cold-worked strip for 1 h at 1300° C followed by water quenching.

Hardness measurements were used to monitor the age-hardening of the three starting conditions as a function of time (up to 1800 h) at temperatures of 400, 500, 600, 700, 800 and 900° C.

Samples for surface examination were prepared by mechanical polishing followed by chemical etching in a mixture of HNO_3 + HCl in the ratio 1 : 5. The etched specimens were examined in a Zeiss optical microscope and a Hitachi S-450 scanning electron microscope, operating at 20 kV with a Link Systems 890 probe microanalyser equipped with a standard ZAF-4 computer program which applied the ZAF (Z = atomic number, A = absorption, F = fluorescence) cor-

0022–2461/84 $03.00 + .12

TABLE I Composition of Elgiloy

Element	mass %*	mass %†
Co	40	41.82
Cr	20	18.64
Ni	15	15.17
Mo	7	7.12
Mn	2	2.20
C	0.115	0.064
Be	0.04	0.038
Fe	15.85	14.95

*Manufacturers' specification – Elgiloy Company, 1565 Fleetwood Drive, Elgin, Illinois 60120, USA.
†Chemical analysis of the 36% cold-worked strip (Acloque Metallurgists Ltd).

rection to the microanalysis data. Carbon extraction replicas of the precipitates in certain heat treated samples were prepared by evaporating a thin layer of carbon on the etched surface of the specimen, which was then made the anode of an electrolytic cell containing dilute HCl as the electrolyte, at a cell voltage of about 5 V. The carbon layer then separated from the specimen surface extracting some precipitates, and was removed from the electrolyte solution using a 200 mesh copper grid which was subsequently washed in distilled water and dried in air.

Thin foils for transmission electron microscopy examination were prepared by jet electro-polishing discs of 3 mm diameter which had been spark machined from the strip. A Metal-Thin double jet automatic electro-thinner was used to electropolish the central part of the disc until a perforation appeared, when a photo-cell terminated the process. 5% perchloric acid in methanol at -25° C was used as the electrolyte at a current of between 40 and 60 mA. After thorough washing in high purity methanol and drying, the foils were examined in a JEOL-JEM100-CX electron microscope, operating at 100 kV, which incorporated a double tilt goniometer stage.

3. Results

3.1. Hardness–time curves

As shown in Fig. 1, the starting hardness of ~ 200 VHN for the ST strip was increased to ~ 340 VHN after 36% cold-reduction (36% CW) and further increased to ~ 440 VHN after 72% cold-working (72% CW).

The subsequent ageing curves for the ST and cold-worked strip in the temperature range 400 to 900° C can be considered in two groups. First, ageing temperatures from 400 to 600° C produced hardening of the cold-worked samples, while the ST strip did not harden significantly in this temperature range. The optimum ageing temperature within this temperature range was 500° C (see Fig. 1).

Second, and in contrast, temperatures from 700 to 850° C produced hardening of the ST specimen at long ageing times (~ 1000 h), while the cold-worked strip did not harden (and indeed softened) in this temperature range. The optimum ageing curves for this group (at 800° C) are shown in Fig. 2. Below 400° C and above 900° C no significant hardening was observed.

3.2. Deformation induced strengthening

It can be concluded from the hardness data in Section 3.1 that the alloy is strengthened by cold-deformation. Fig. 3 compares the optical micrographs of the alloy before (ST) and after 36% and 72% cold-deformation. It can be seen that the microstructure of ST strip consists of equiaxed grains with a number of annealing twins, whereas the 36% CW and 72% CW structures contain, in addition, bands of fine striations (deformation bands) which form networks in some regions.

The homogenized structure of the ST strip contains some dissociated dislocations as seen from the transmission electron micrograph of Fig. 4a and is f c c, as determined from the selected area diffraction pattern of Fig. 4b, as well as by X-ray diffraction analysis which gave a value of $a = 0.3596$ nm for the matrix lattice parameter.

The main feature of the highly deformed structures of the 36% CW and 72% CW strips is the existence of deformation bands as shown in the TEM micrographs of Fig. 5, which are thought to be related to the fine striations observed in the optical micrographs of Fig. 3.

Electron diffraction patterns from these areas of the cold-worked samples consist of complex, composite patterns from both the f c c matrix and the thin platelets as shown in Fig. 5b, where the less intense spots come from the thin platelets and the main bright spots are matrix spots. This can be confirmed by dark field techniques, as shown in Fig. 5d, where the platelets are revealed in the high resolution dark field (HRDF) image, and Fig. 5e which is a matrix dark field micrograph. Difficulties are encountered in the interpretation and indexing of these diffraction patterns, as in many cases the patterns from the platelets

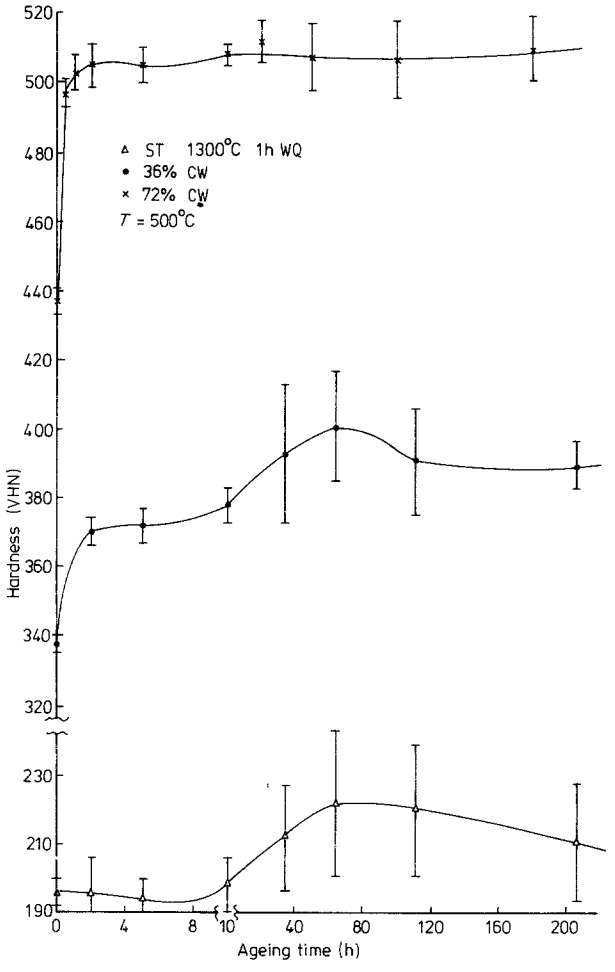

Figure 1 Ageing curves for ST, 36% CW and 72% CW strips at 500° C.

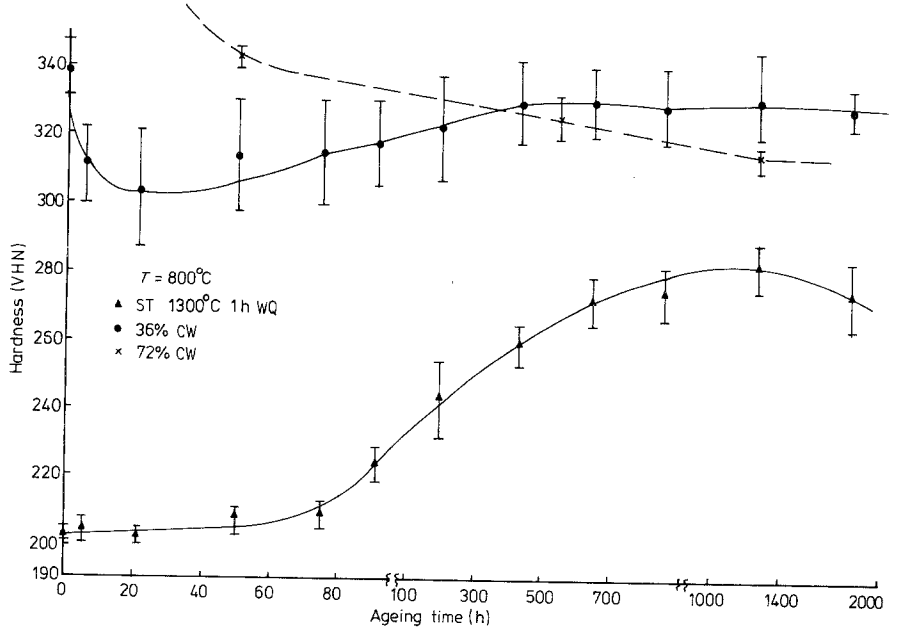

Figure 2 Ageing curves for ST, 36% CW and 72% CW strips at 800° C.

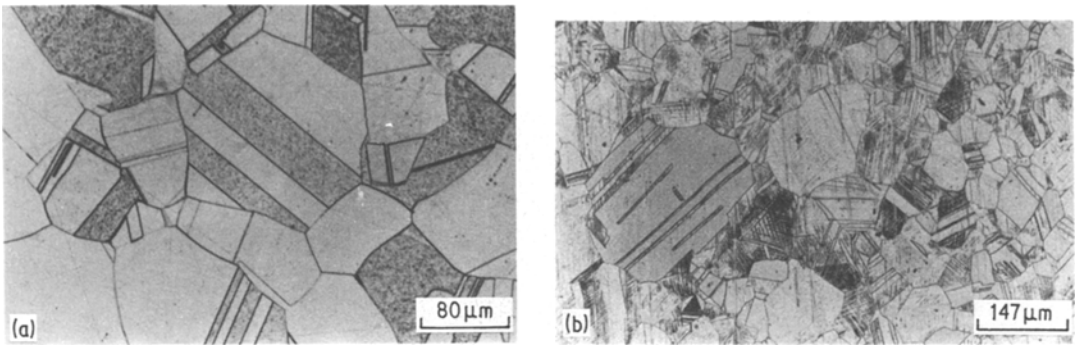

Figure 3 Optical micrographs (a) ST; (b) 36% CW; (c) 72% CW.

can be indexed either as a f c c mechanical twin or as a h c p ϵ-phase. Identification from the bright field and dark field micrographs is not possible either, because of the very smimilar morphologies of the mechanical micro-twins and the h c p ϵ-platelets. Hence structure identification requires the application of diffraction analysis techniques as discussed in the following section.

3.2.1. Electron diffraction analysis of thin platelets

Kestenbach [5] has analysed the electron diffraction patterns of thin twins and h c p platelets in an f c c matrix by constructing composite diffraction patterns using three-dimensional reciprocal lattice models, given by Pashley and Stowell [6], for both f c c-twin and f c c–h c p structure combinations. The composite patterns demonstrated that, in many low order matrix orientations, unambiguous distinction between an f c c twin and an h c p crystal structure of the same habit is not possible.

In the case of thin platelets (both h c p and micro-twins), the diffracted intensity distribution in reciprocal space is extended into streaks perpendicular to their habit planes, causing a continuous change in the position of the diffracted spots during specimen tilting. This intensity streaking, combined with double diffraction, and the fact that more than one platelet habit may contribute to the diffraction pattern, makes the determination of orientation using the thin platelets very difficult. This difficulty can be overcome by using the matrix reflections for the determination of the

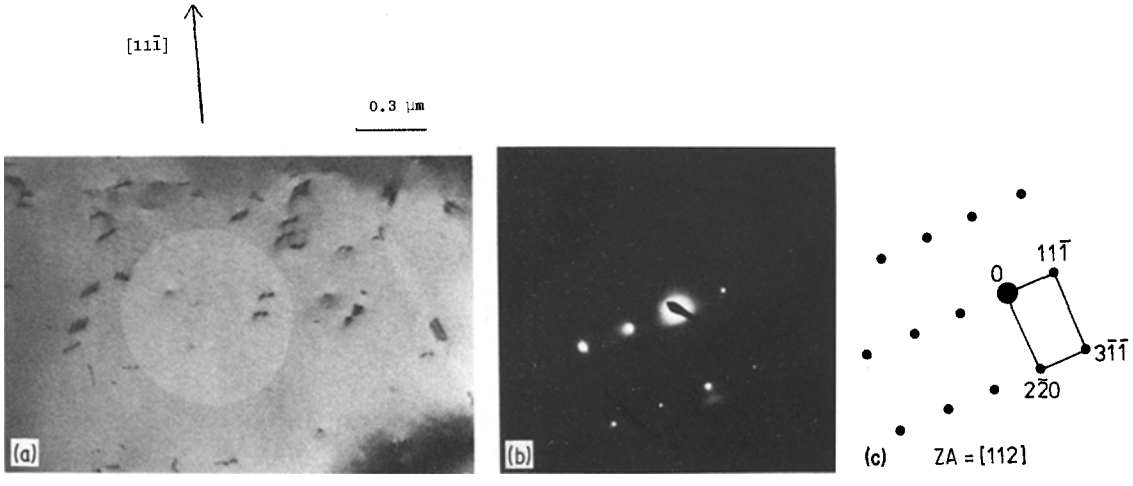

Figure 4 ST strip (a) bright field; (b) SAD pattern of (a); (c) key to (b).

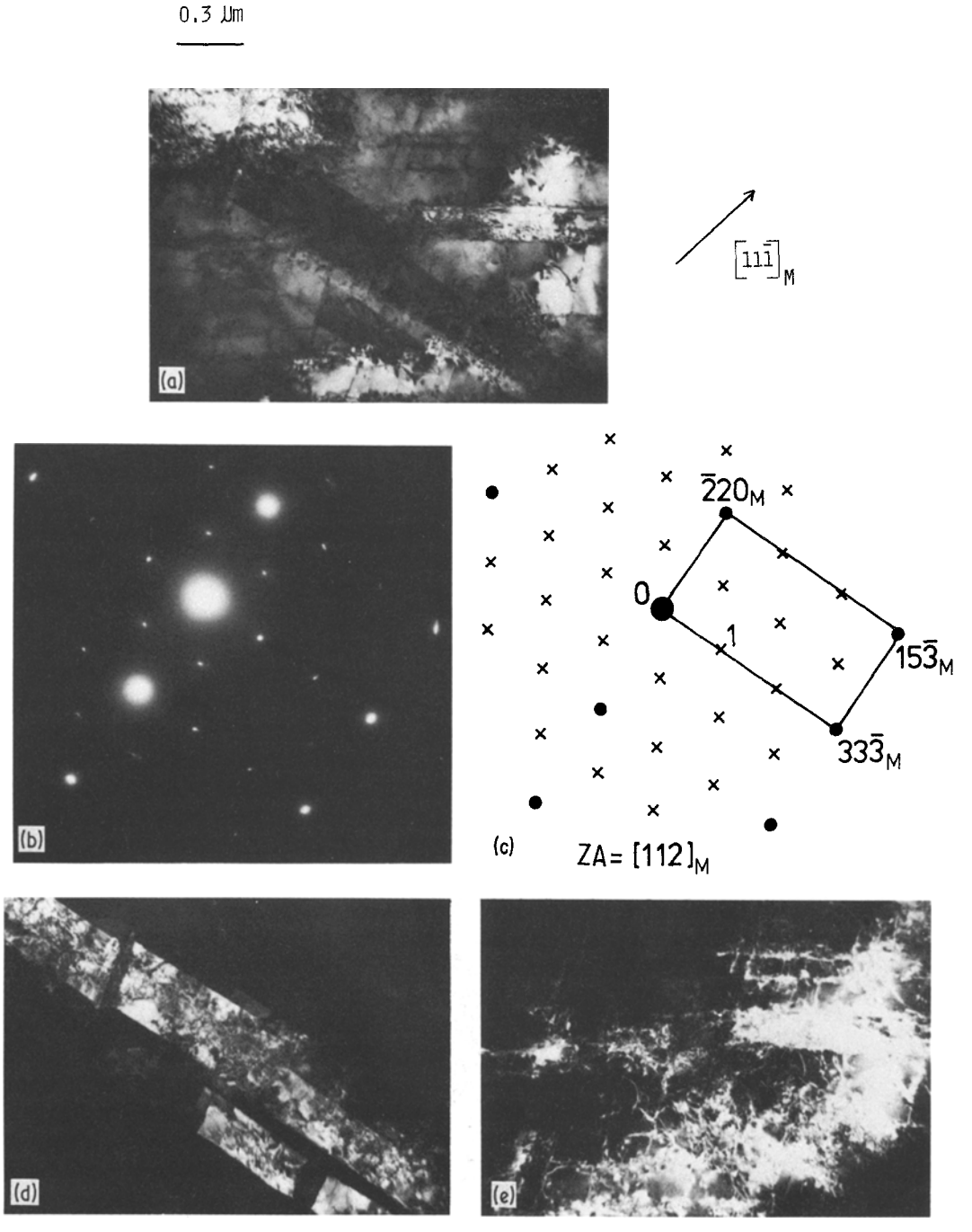

Figure 5 36% CW strip (a) bright field; (b) SAD pattern of (a); (c) key to (b): ZA = $[1\,1\,2]_M$; • matrix (M); × platelets. (d) High resolution dark field (HRDF) using platelet reflection 1. (e) HRDF using $(\bar{2}\,2\,0)_M$ matrix reflection.

beam orientation since, except for very thin foil areas, the diffracted intensity from the matrix is confined to the vicinity of the reciprocal lattic nodes (i.e. there is little streaking of matrix spots).

A survey of orientations in which twins and h c p platelets may or may not be distinguished was considered by Kestenbach, which is given in Table II, and shows that no distinction is possible if the beam enters the matrix along ⟨1 0 0⟩, ⟨2 1 1⟩ or ⟨3 1 0⟩ directions. In this case, and for all the variants of other orientations referred to in the last column of Table II, twins and h c p electron diffraction patterns are identical and overlap on matrix spots. Thus, the composite diffraction

TABLE II Exact orientations in which electron diffraction can or cannot distinguish between twin and hcp plates of (1 1 1)-habit in fcc matrix, after Kestenbach [5]

Beam direction $\langle h\,k\,l\rangle$ in matrix	Total number of variants*	Variants $h\,k\,l$ in which distinction is possible	Number of variants* in which distinction is impossible
1 1 0	6	$1\bar{1}0, 10\bar{1}, 01\bar{1}$	3
1 0 0	3	–	3
2 1 1	12	–	12
3 1 0	12	–	12
1 1 1	4	1 1 1	3
3 2 1	24	3 2 1, 3 1 2, 2 3 1 2 1 3, 1 3 2, 1 2 3 $\bar{3}\,2\,1, \bar{3}\,1\,2, 2\,\bar{3}\,1$ $2\,1\,\bar{3}, 1\,\bar{3}\,2, 1\,2\,\bar{3}$	12
4 1 1	12	4 1 1, 1 4 1, 1 1 4	9
2 1 0	12	2 1 0, 2 0 1, 1 2 0 1 0 2, 0 2 1, 0 1 2	6
2 2 1	12	$2\,2\,\bar{1}, 2\,\bar{1}\,2, \bar{1}\,2\,2$	9
5 1 1	12	$5\,\bar{1}\,\bar{1}, \bar{1}\,5\,\bar{1}, \bar{1}\,\bar{1}\,5$	†
5 2 1	24	$5\,2\,\bar{1}, 5\,\bar{1}\,2, 2\,5\,\bar{1}$ $2\,\bar{1}\,5, \bar{1}\,5\,2, \bar{1}\,2\,5$	†
7 4 1	24	7 4 1, 7 1 4, 4 7 1 4 1 7, 1 7 4, 1 4 7	†

*Positive or negative sense of direction neglected.
†Not determined.

patterns are the same as the matrix pattern alone. For all the other cases in which twin and hcp platelets may be distinguished, the composite diffraction patterns are given in Figs. 6a, b and c, according to whether the extra low-order diffraction spots are due to twin orientations, hcp phase, or both structures, respectively.

It should be noted that the indexing of the $(\bar{1}\,2\,5)_M$ orientation in Fig. 6b by Kestenbach, for both the matrix and hcp diffraction spots, is incorrect, and these indices have been marked with a cross (X). The pattern has been reindexed in a self-consistent manner and the correct indices are printed on the pattern in Fig. 6.

3.2.2. Analysis of the TEM results for 36% CW and 72% CW strip

The double tilt specimen stage of the transmission electron microscope was used in order to generate a large number of electron diffraction patterns corresponding to various electron beam directions. A selection of the results with electron beam directions in which distinction between a mechanical microtwin and an hcp platelet is possible are described in the following section.

An example of a composite electron diffraction pattern for fcc matrix–fcc twins–hcp platelets, for the 36% CW strip is shown in Fig, 7, for a $(0\,1\,2)_M$ matrix orientation. The platelets of Figs. 7a and 7d can be identified as fcc twins, using the electron diffraction pattern in Fig. 7b (compare to Fig. 6c).

Identification of the hcp ϵ-platelets in the 36% CW samples was achieved by analysing the composite electron diffraction pattern in the $(\bar{1}\,2\,5)_M$ matrix orientation as shown in Fig. 8. The electron diffraction pattern of Fig. 8b is identical to the one proposed in Fig. 6b, and can be indexed accordingly. The high resolution dark field micrograph of Fig. 8d reveals the structure of the hcp ϵ-platelets in the 36% CW strip. The identification of the hcp ϵ-platelets was further confirmed by tilting to the $(1\,1\,1)_M$ matrix orientation (remaining in the same region of the foil), as shown in Fig. 9, where the typical orientation relationship, $(1\,1\,1)_{fcc}\|(0\,0\,0\,1)_{hcp}$, was exhibited (compare to Fig. 6b).

For the 72% CW strip, the $(1\,4\,7)_M$ matrix orientation revealed the presence of the hcp ϵ-platelets as shown in Fig. 10 (compare to Fig. 6b) for which a large number of hcp ϵ-platelets can be seen in the high resolution dark field image.

The fcc twins were also detected in some areas of the 72% CW foil as revealed in Fig. 11, with the diffraction pattern indicating a $(1\,1\,4)_M$ matrix orientation (compare to Fig. 6a).

X-ray diffractometer traces for the 36% CW and 72% CW strip did not detect the presence of hcp ϵ-phase. and only matrix reflections were obtained which gave lattice parameter values of 0.3589 nm and 0.3592 nm for the 36% CW and 72% CW samples, respectively.

3.3. Ageing induced strengthening at 500° C

Ageing curves for the ST, 36% CW and 72% CW strips shown in Fig. 1 indicate that the peak hardness is achieved after about 2 h of ageing at 500° C for the 72% CW condition, whereas for the ST and 36% CW strips it is obtained after about 64 h.

The hardening of the ST strip at 500° C is not significant and the microstructure after 64 h of ageing is essentially the same as that of the ST strip shown in Figs. 3 and 4.

Age hardening of the cold-worked strip (36% CW and 72% CW) at 500° C was substantial. The microstructures were examined for various ageing times (5, 64, 100, and 500 h), and, for all the

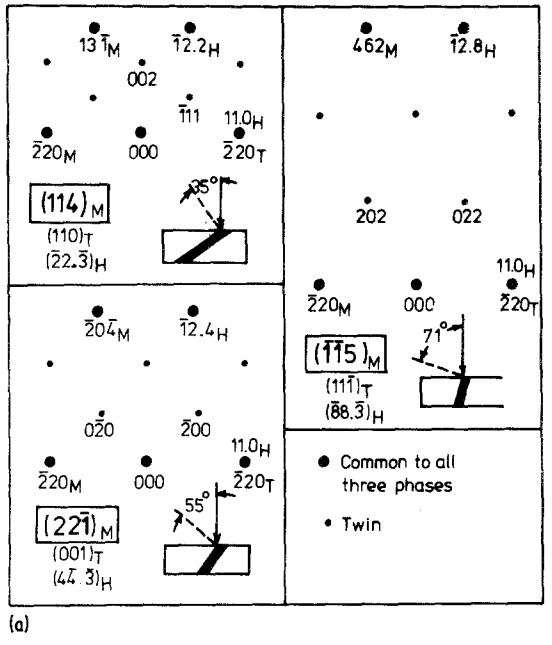

(a)

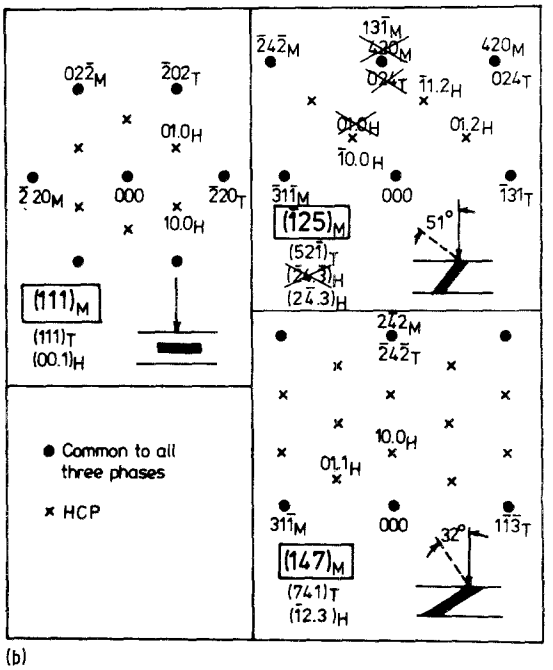

(b)

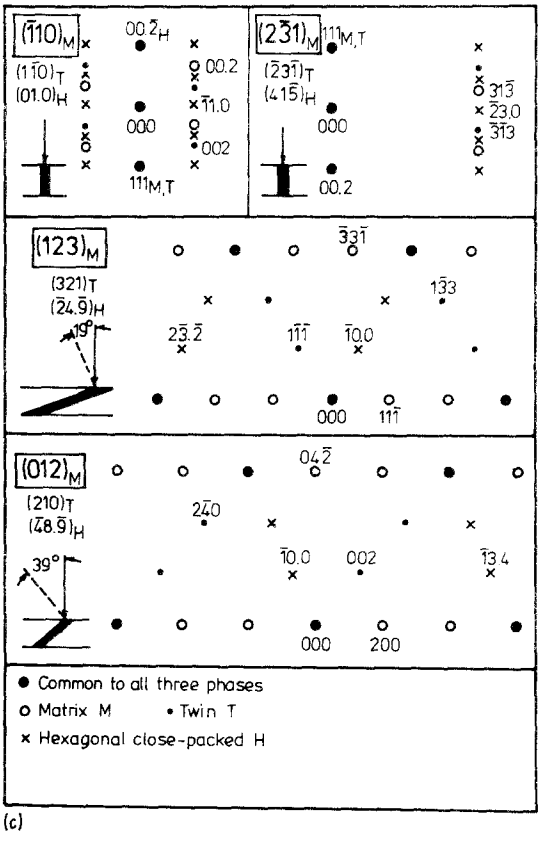

(c)

Figure 6 (a) Composite f c c-twin-h c p electron diffraction patterns with extra spots due to twinning on (1 1 1) matrix planes. Indices in parentheses refer to reciprocal lattice planes. Plate orientation in foil indicated by angle between incident beam and plate normal. After Kestenbach [5]. (b) Composite f c c-twin-h c p electron diffraction patterns with extra spots due to h c p plates on (1 1 1) matrix planes. Plane indices and plate orientation as in Fig. 6a. After Kestenbach [5]. (c) Composite f c c-twin-h c p electron diffraction patterns with extra spots due to twinning and h c p plates on (1 1 1) matrix planes. Planes indices and plate orientation as in Fig. 6a. Double diffraction effects not included. After Kestenbach [5].

ageing times examined, the main feature noted was again the existence of thin platelets, both of f c c twins and of h c p ϵ-phase, similar to the microstructures prior to ageing. An example of an f c c twin platelet in the 36% CW, aged 64 h at 500° C (peak hardness), is shown in Fig. 12 (compare to Fig. 6a), and an example of h c p ϵ-platelets in 72% CW, aged 5 h at 500° C (peak hardness) is shown in Fig. 13 (compare to Fig. 6b).

In addition to the presence of h c p ϵ-phase and f c c twin platelets, diffraction streaks or "relrods" were observed in certain matrix orientations of the cold-worked and aged at 500° C samples, from which further platelet structures were revealed using dark field images as shown in Figs. 14 and 15, for the 36% CW aged 5 h at 500° C and 72% CW aged 5 h at 500° C conditions, respectively.

One other feature noted was the appearance of some diffraction rings in certain regions of the cold-worked and aged at 500° C samples, as shown in Fig. 16 for a 72% CW sample aged 5 h at 500° C. High resolution dark field micrographs from these

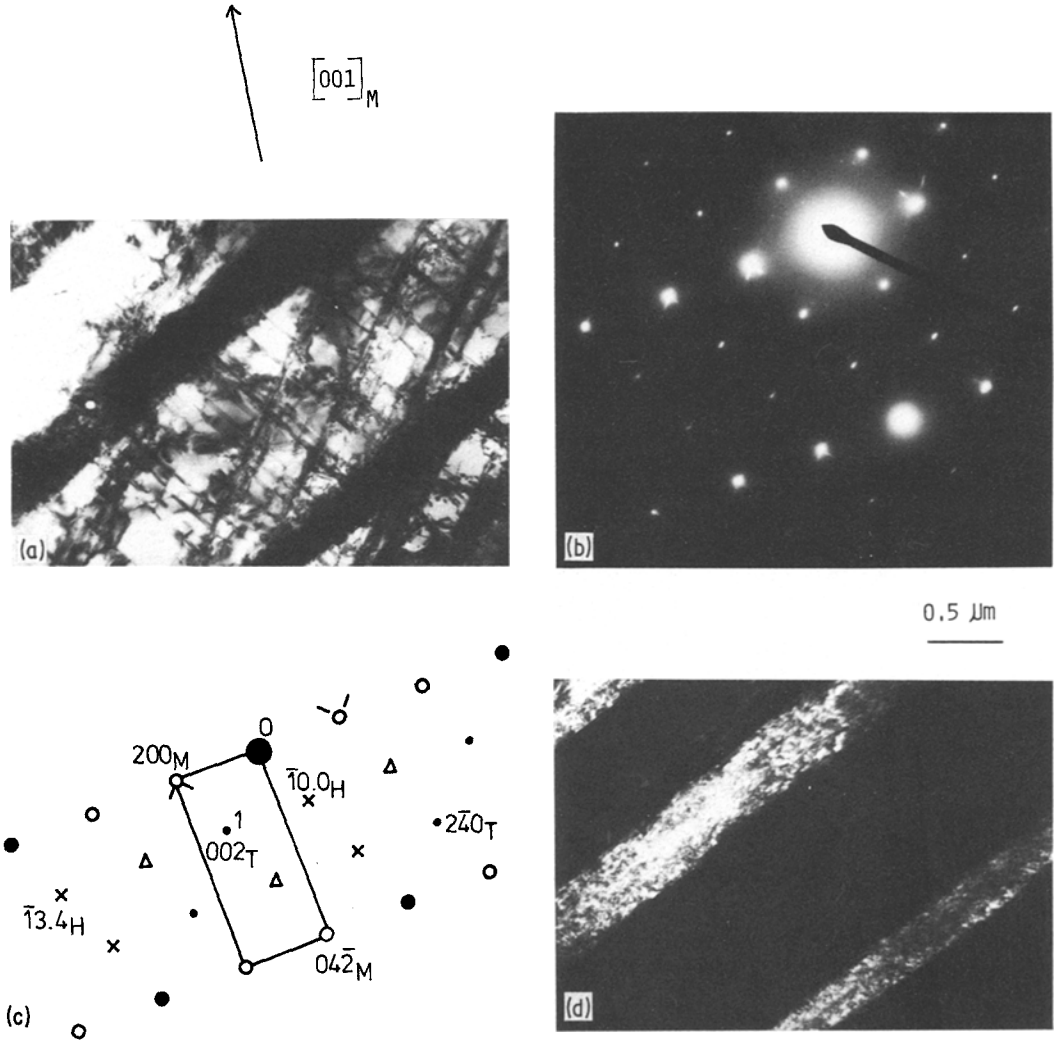

Figure 7 36% CW strip (a) bright field; (b) SAD pattern of (a), with a $(0\,1\,2)_M$ matrix orientation; (c) key to (b). • Common to all three phases; ○ matrix (M); · twin (T); × h c p (H); △ double diffraction; ZA = $[0\,1\,2]_M = [2\,1\,0]_T = [\bar{4}\,8{\cdot}\bar{9}]_H$. (d) HRDF, using spot 1 (i.e. $0\,0\,2_T$), showing f c c twin platelets.

rings reveal the presence of very "fine" particles as can be seen in Figs 16d. It was thought that these rings are those referred to by Henmi *et al.* [3] as produced by "fine" α-cobalt (i.e. h c p phase of cobalt) particles precipitated during ageing of the cold-rolled Elgiloy at 500° C. In fact, the rings can be attributed to metal oxide contamination formed as "fine" particles on the surface of some of the foils, during the electropolishing operation. This can be seen from Table III, in which the *d*-spacings of the rings are compared to those of some metallic oxides.

TABLE III Diffraction ring *d*-spacings, measured from Fig. 16b (for the 72% CW strip aged 5 h at 500° C), together with some metallic oxide *d*-spacings (from ASTM cards) given for comparison

Ring number	d_{ring}(nm)	*d* (nm) of some metallic oxides (from ASTM)			
		$NiFe_2O_4$	$CoO{\cdot}Fe_2O_3$	$NiCr_2O_4$	$FeCoCrO_4$
1	0.305	0.295	0.297	0.295	0.295
2	0.251	0.251	0.253	0.253	0.246
3	0.209	0.209	0.208	0.206	0.207
4	0.162	0.161	0.161	0.162	0.168
5	0.151	0.148	0.148	0.147	0.147

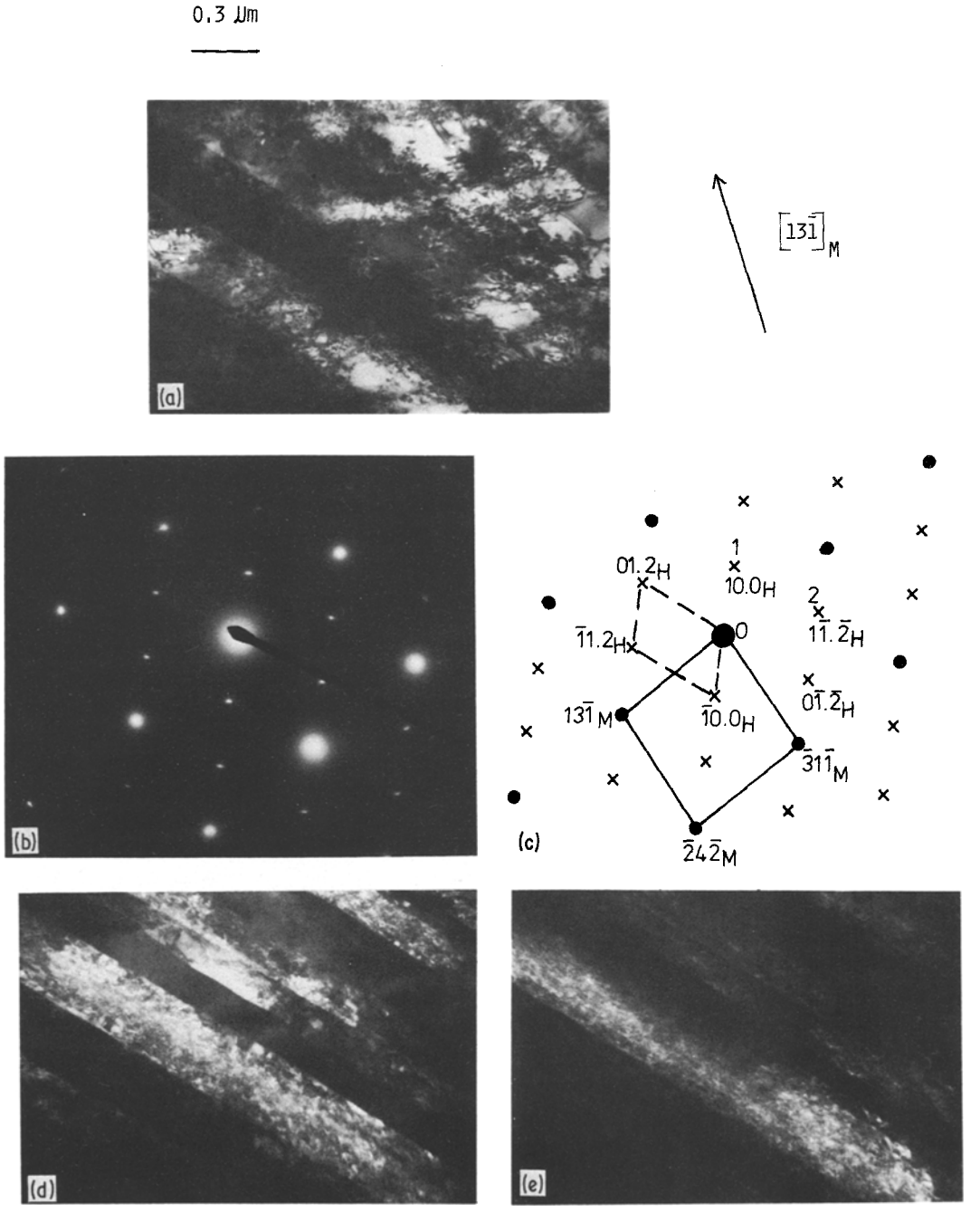

Figure 8 36% CW strip (a) bright field; (b) SAD pattern of (a), with a $(\bar{1}\,2\,5)_M$ matrix orientation; (c) key to (b). • Common to all three phases; × h c p; ZA = $[\bar{1}\,2\,5]_M = [2\bar{4}\cdot 3]_H$. (d) and (e) HRDF, using spot 1 (i.e. $1\,0\cdot 0_H$) and spot 2 (i.e. $1\,\bar{1}\cdot\bar{2}_H$), respectively, showing h c p ϵ-platelets.

X-ray diffractometer traces of the cold-worked and aged at 500° C samples did not detect the presence of any second phase and only f c c matrix reflections were present, with lattice parameter values of 0.3587 and 0.3591 nm for the 36% CW aged 64 h at 500° C and 72% CW aged 5 h at 500° C strips, respectively.

3.4. Ageing at 800° C

Ageing cold-worked samples (both 36% CW and

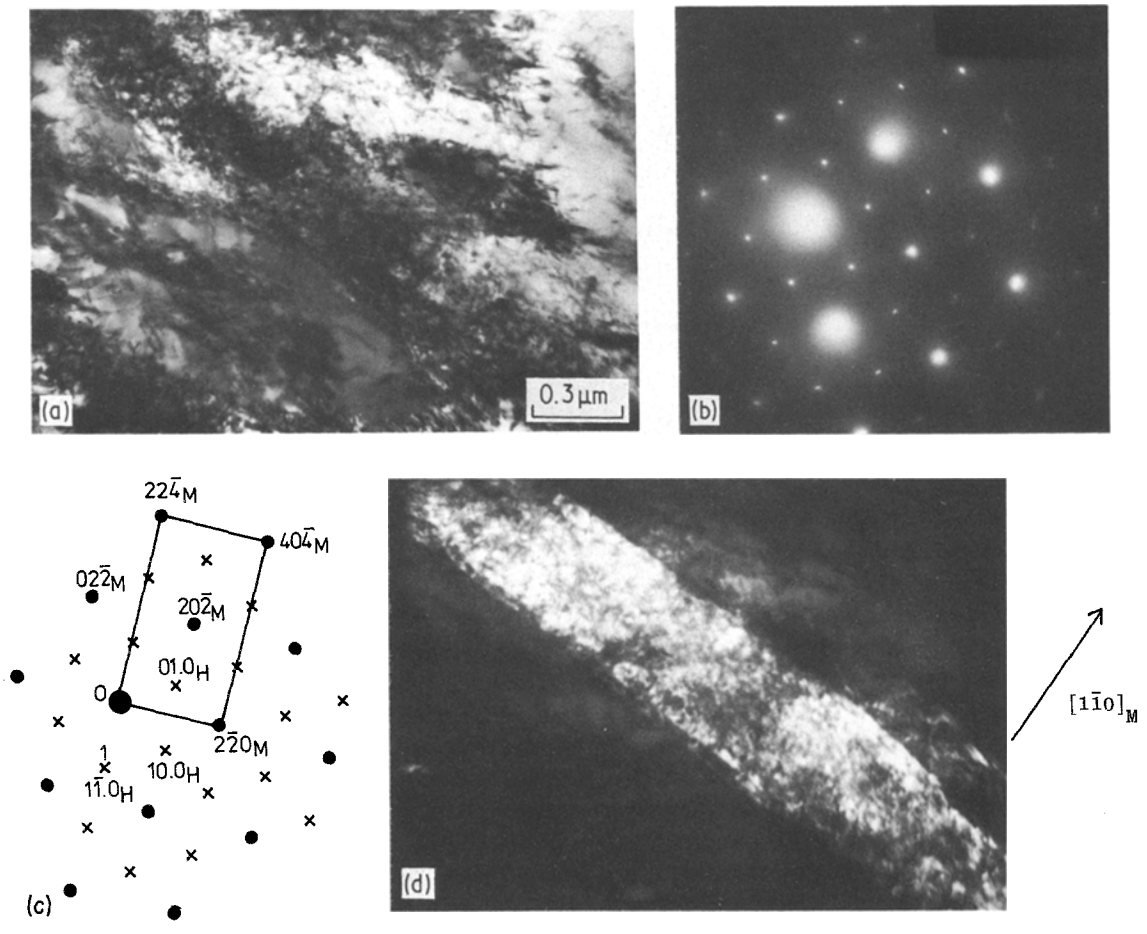

Figure 9 36% CW strip. Same region as Fig. 8, but tilting to $(1\,1\,1)_M$ matrix orientation; (a) bright field; (b) SAD pattern of (a), with a $(1\,1\,1)_M$ matrix orientation; (c) key to (b). • Common to all three phases; × h c p; ZA = $[1\,1\,1]_M$ = $[0\,0\cdot1]_H$ $(1\,1\,1)_{f\,c\,c} \| (0\,0\cdot1)_{h\,c\,p}$. (d) HRDF, from spot 1 (i.e. $1\,\bar{1}\cdot0_H$), showing h c p ϵ-platelets.

72% CW) at 800° C produced softening, with the reduction in hardness being more pronounced for the 72% CW condition. In contrast the ST strip age-hardens at 800° C after long ageing times with the peak hardness reached after 1263 h at this temperature as shown in Fig. 2.

Optical micrographs of the ST, aged 1814 h at 800° C condition, reveal the presence of a second phase both within the grains and at the grain boundaries forming a continuous network in some regions (Fig. 17). The amount of this precipitate was estimated to be about 15% by volume with the particle size ranging from 1 to 8 μm, as seen in Fig. 18. The precipitate was also observed in the cold-worked strip after prolonged ageing at 800° C, but clustering of the precipitates had occurred at twin boundaries and deformation band sites as shown in Fig. 19, with the precipitates varying from 1 to 3 μm in size.

Carbon extraction replicas of the precipitates (Fig. 20) were analysed qualitatively using TEMSCAN and quantitatively using SEM probe microanalysis and the results are shown in Fig. 21 and Table IV, respectively. Two types of precipi-

TABLE IV SEM electron probe quantitative microanalysis for ST aged 1814 h at 800° C samples, using Link Systems 890 probe microanalyser with ZAF4 computer program (small carbon content ignored)

Element	Matrix analysis of bulk ST sample (wt % ± 2)	Analysis of extracted precipitates (wt % ± 2)	
		Precipitate 1 (majority)	Precipitate 2 (minority)
Co	40	30	16
Cr	20	13	49
Ni	16	5	4
Mo	7	45	26
Fe	15	6	4
Mn	2	1	1

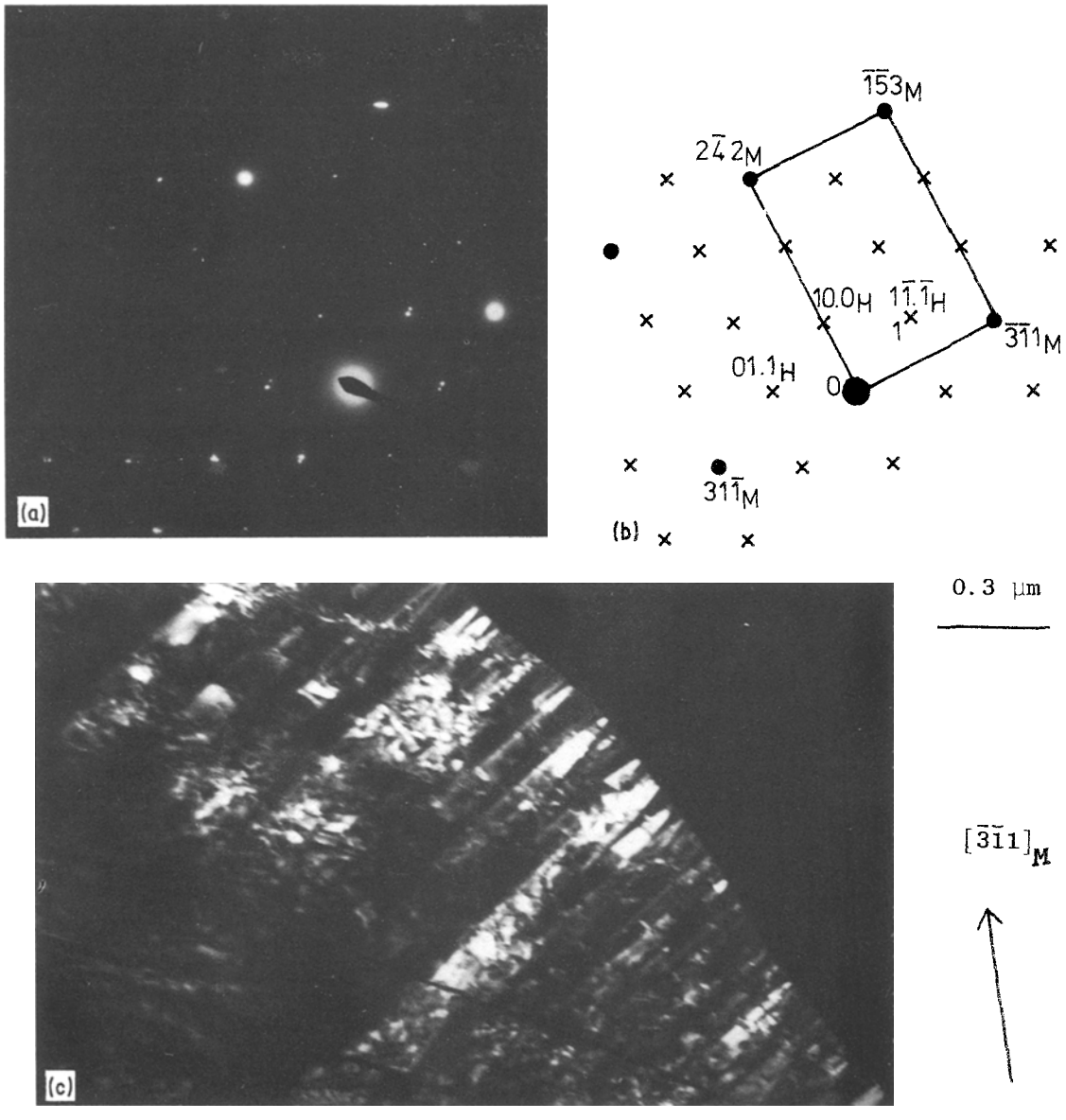

Figure 10 72% CW strip (a) SAD pattern of (c), with a $(1\,4\,7)_M$ matrix orientation; (b) key to (a). • Common to all three phases; × hcp; ZA = $[1\,4\,7]_M = [\bar{1}\,2\cdot 3]_H$. (c) HRDF, using spot 1 (i.e. $1\,\bar{1}\cdot\bar{1}_H$), showing a number of hcp ϵ-platelets.

tates were detected from these results, the majority (type 1) being mainly rich in molybdenum, cobalt and chromium, with small amounts of iron and nickel, and the minority (type 2) which were fewer in number and are rich in chromium and molybdenum, with small amounts of cobalt, nickel and iron. Visual distinction between the two precipitates, however, could not be made due to their similar morphologies.

Most of the precipitates were too thick to be electron transparent and electron diffraction patterns could not be formed. However, in some areas of the foil samples, diffraction patterns from the matrix and some "thin" precipitates could be obtained as shown in Fig. 22. The "thin" precipitate diffraction spots can be indexed as fcc with a lattice parameter 3 times that of the matrix, and an orientation relationship given by:

$$\{0\,0\,1\}\text{ppt}\|\{0\,0\,1\}\text{matrix}$$
$$\langle 1\,1\,0\rangle\text{ppt}\|\langle 1\,1\,0\rangle\text{matrix}$$

As the lattice parameter of the matrix is about

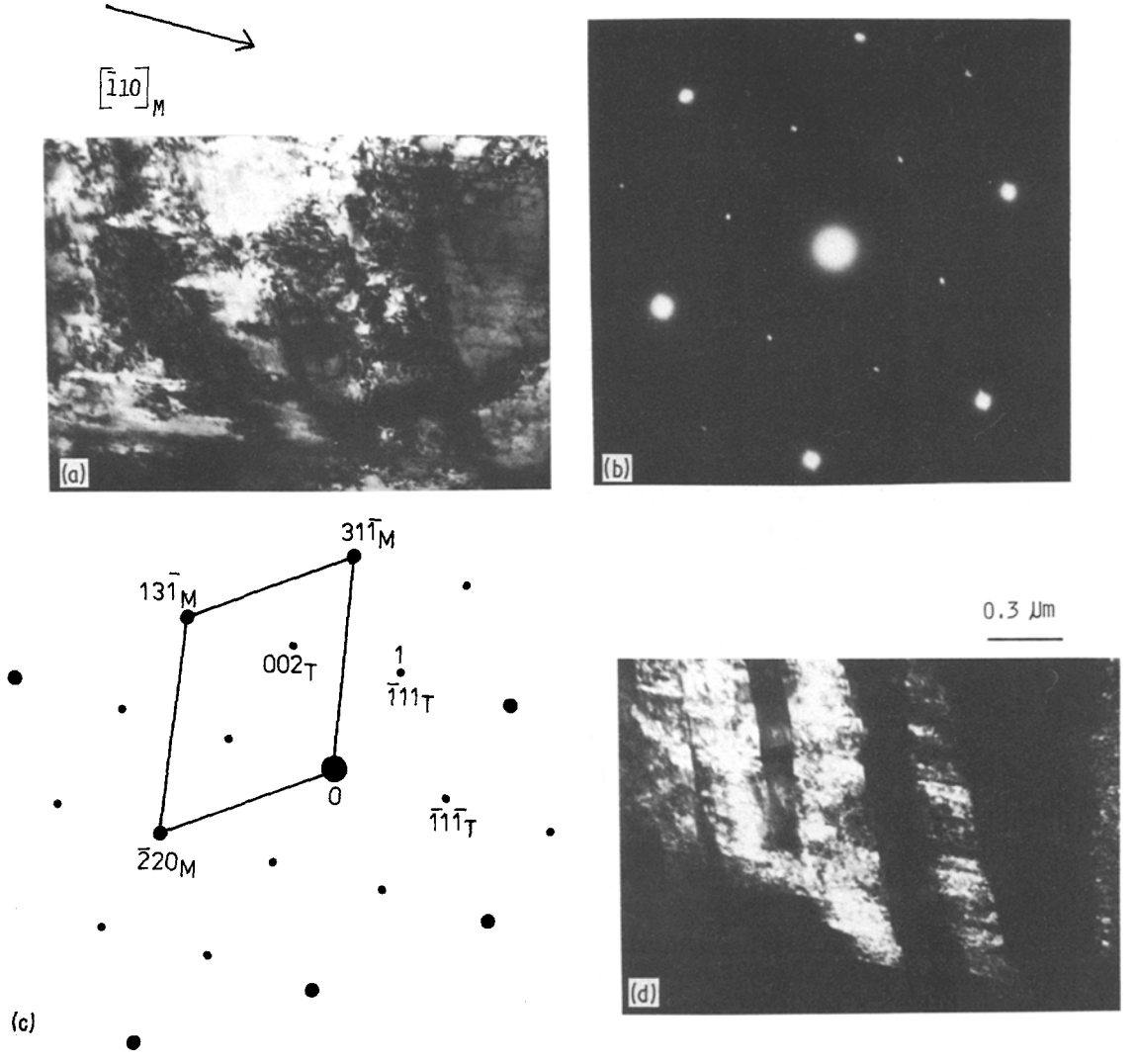

Figure 11 72% CW strip (a) bright field; (b) SAD pattern of (a), with a $(1\,1\,4)_M$ matrix orientation; (c) key to (b). • Common to all three phases; · twin; $ZA = [1\,1\,4]_M = [1\,1\,0]_T$. (d) HRDF, using spot 1 (i.e. $\bar{1}\,1\,1_T$) showing fcc twin platelets.

0.359 nm, that of the thin precipitate will be ~ 1.08 nm, which is close to that of $M_{23}C_6$ carbides [7]. This result is in agreement with the microprobe analysis data for the minority precipitate (type 2) in Table IV and Fig. 21.

X-ray diffractometer traces of the aged at 800° C strips contained precipitate reflections in addition to matrix reflections and these results are given in Table V, together as a comparison, with the *d*-spacings of a Co–Mo–Cr precipitate (last column) reported by Lux and Bollmann [8], for a heat treated Co–Cr–Mo alloy. It should be pointed out, however, that Lux and Bollmann's data were from extracted precipitates, whereas the present results are from precipitates within the matrix. Nevertheless the agreement between the two sets of data is reasonable and confirms the microprobe analysis data given for the majority precipitates (type 1) in Table IV and Fig. 21.

4. Discussion

Hardening of the Elgiloy ST strip by cold-working was accompanied by the formation of a network of striations or platelets, composed of either fcc deformation twins and/or the hcp ϵ-phase. Although such platelets have not been previously noted in Elgiloy, they have been widely reported in similar cobalt-based alloys such as the multiphase (MP) alloys [9–13] as well as in stainless steels [14–17]. For MP alloys the structure at high

TABLE V X-ray data for ST plus aged 1814 h at 800° C strip, together with the *d*-spacings of a CoCrMo precipitate, given by Lux and Bollmann [8]

ST + aged 1814 h at 800° C strip			CoCrMo precipitate, Lux and Ballmann [8]
Peak number	θ°	*d*(nm)	*d*(nm)
1	19.05	0.236	0.236
			0.227
2	20.70	0.218	0.218
3	21.08	0.214	0.214
4	21.40	0.211	0.210
5(1 1 1) matrix	21.91	0.207	0.205
6	22.34	0.203	0.203
7	22.78	0.199	0.199
8	23.48	0.194	0.194
9(2 0 0) matrix	25.48	0.180	0.193, 0.187, 0.177
			0.171, 0.159, 0.157, 0.149
			0.142, 0.138, 0.136, 0.134
10	36.08	0.131	0.132, 0.130
11	36.80	0.129	0.128
12(2 2 0) matrix	37.53	0.127	0.127
			0.125, 0.124, 0.122, 0.121
			0.118
13(3 1 1) matrix	45.53	0.108	
14(2 2 2) matrix	48.21	0.103	

a_{matrix} (at $\theta = 90^\circ$) = 0.3587 nm.

temperature is α-f c c, whereas at low temperatures the ϵ-h c p phase is stable. The f c c → h c p transformation, however, is very sluggish and does not occur by cooling below the lower transformation temperature. The α-f c c structure then exists as a metastable phase at room temperature. The transformation from f c c to h c p ($\alpha \rightarrow \epsilon$), however, can be brought about by mechanical deformtion, and the extent of the transformation, which is martensitic, depends on the amount of deformation imposed. The strengthening of the MP alloys by cold-working was originally attributed to the formation of the h c p ϵ-platelets at room temperature [9–11, 18]. Raghavan *et al.* [12], on the other hand, considered the platelets which formed during cold-deformation of MP35N alloy to be f c c deformation twins and not h c p ϵ-phase. In agreement with this conclusion, Michels *et al.* [18] reported the formation of f c c deformation twins in an Fe–25% Ni–21% Co–20% Cr–8% Mo alloy cold drawn up to 75%. It was argued that the similarity in morphology between the h c p ϵ-phase and f c c deformation twins was responsible for the false identification of f c c deformation twins as h c p ϵ-platelets in MP alloys. More recently, however, Gonzalez De Armengol [13] examined this in an MP35N alloy and argued that the formation of h c p ϵ-phase or f c c deformation twins was dependent on the amount as well as the temperature of deformation.

In the present work, some of the platelets in the cold-worked Elgiloy (both 36% CW and 72% CW) were identified as h c p ϵ-phase, whereas others were determined to be f c c deformation twins, i.e. both ϵ-h c p phase and f c c deformation twins are considered to coexist after 36% and 72% room temperature cold-deformation in Elgiloy.

The age-hardening behaviour of Elgiloy shown in Fig. 1 is in general agreement with previous findings [1, 3, 4], but the present microstructural data do not support the previous proposals as to the mechanism of this hardening.

Trickey's [1] suggestion that Elgiloy precipitation hardens in the same manner as copper–beryllium is not compatible with the present findings, as the continuous precipitation sequence of GP zones $\rightarrow \gamma' \rightarrow \gamma$ and the discontinuous precipitation processes reported for the Cu–Be [23–25] were not observed in Elgiloy. Henmi *et al.* [3] attributed the age-hardening of cold-worked Elgiloy at 500° C to the precipitation of very "fine" α-cobalt particles, but as described in a previous section, their supporting experimental observation can be attributed to oxide contamination.

Legendre and Wache [4] attributed the age-hardening of cold-deformed Phynox (an alloy of practically the same composition as Elgiloy, with composition in wt%, 0.12% C, 0.21% Si, 0.008% S, 0.013% P, 1.68% Mn, 16.01% Ni, 20.16% Cr, 6.33% Mo, 39.7% Co, balance Fe), at 500° C to a disorder → order transformation, but, in common with the previous studies of age-hardening of cold-worked Elgiloy, did not consider the presence of deformation twins and h c p ϵ-platelets induced by cold-deformation prior to ageing.

Streaks or "relrods" were observed in the SAD pattern of the cold-rolled Elgiloy samples aged at 500° C, from which thin platelets were revealed. In the case of "thin" platelets (deformation microtwins or h c p ϵ-phase), the diffracted intensity distribution in reciprocal space is extended into streaks perpendicular to their habit planes.

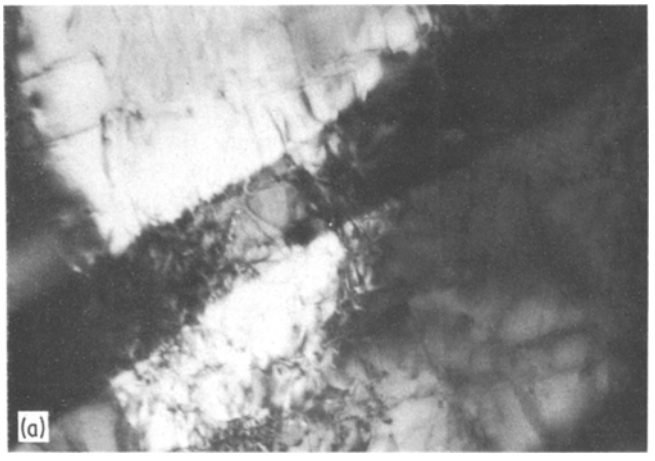

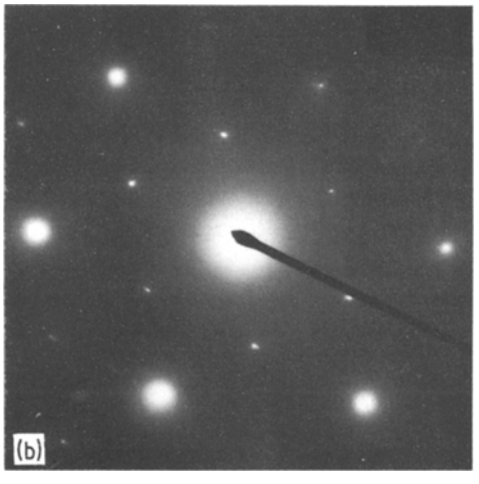

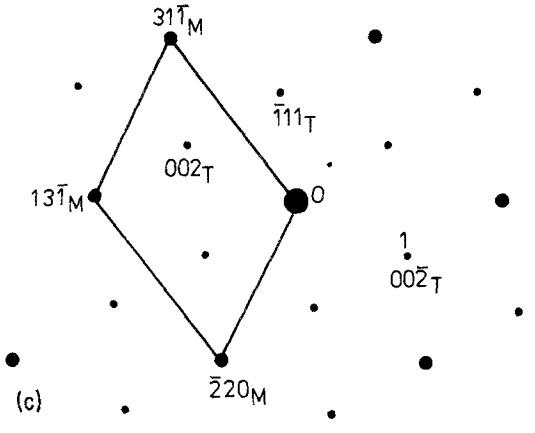

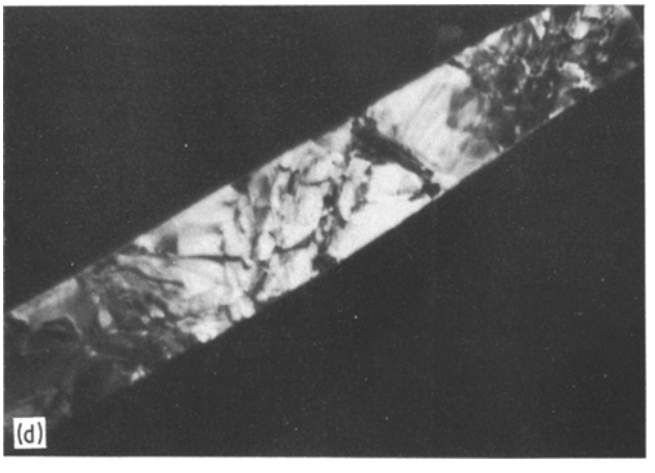

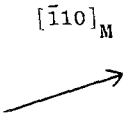

Figure 12 36% CW strip, aged 64 h at 500° C (peak hardness): (a) bright field; (b) SAD pattern of (a), with a $(1\,1\,4)_M$ matrix orientation; (c) key to (b). • Common to all three phases; · twin; ZA = $[1\,1\,4]_M = [1\,1\,0]_T$. (d) HRDF, from spot 1 (i.e. $0\,0\,\bar{2}_T$), showing an f c c twin platelet.

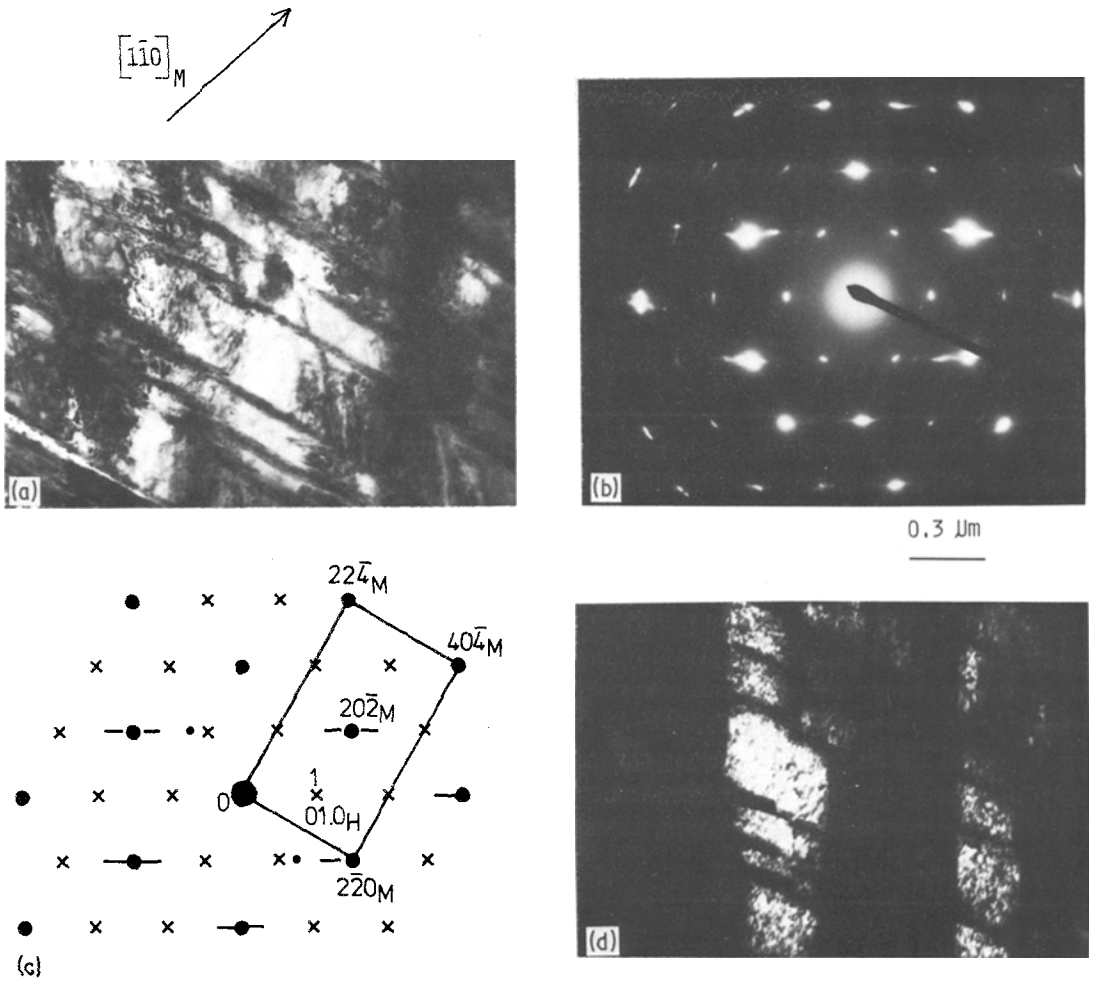

Figure 13 72% CW strip, aged 5 h at 500° C (peak hardness): (a) bright field; (b) SAD pattern of (a), with a $(1\,1\,1)_M$ matrix orientation; (c) key to (b). • Common to all three phases; × h c p; ZA = $[1\,1\,1]_M = [0\,0\cdot1]_H$. $(1\,1\,1)_{fcc} \| (0\,0\cdot1)_{hcp}$. (d) HRDF, from spot 1 (i.e. $0\,1\cdot0_H$), showing h c p ϵ-platelets.

So, if the thick dimension of the plate (i.e. the habit plane) is parallel to the electron beam (and the thin dimension is therefore perpendicular to it), streaks will be recorded on the diffraction pattern. Consequently, although precipitation of two-dimensional zones (perhaps as a precursor of the Mo–Co–Cr compound) could produce the same effect, observations of "relrods" from the thin platelets are not sufficient to establish the existence of segregated zones within these regions, although zone formation has been identified in related alloys [9, 11, 26]. Continued prolonged ageing (up to 1000 h) of the cold-worked strip at 500° C did not resolve this point as the separation of a three-dimensional precipitate was not initiated.

It is possible that further h c p ϵ-platelets are formed during ageing of the cold-worked Elgiloy at 500° C, similar to those reported in MP alloys [12, 13] for which ageing of the cold-worked samples in the (f c c + h c p) region was thought to accelerate the $\alpha_{fcc} \rightarrow \epsilon_{hcp}$ transformation, but the ϵ-phase density was not quantified and will be the subject of further study.

Ageing of the cold-worked strips at 800° C leads to softening which is attributed to both the transformation of the deformation induced h c p ϵ-platelets to the f c c phase (as f c c is stable at high temperature) and the annihilation of lattice defects produced by recovery and recrystallization. Ageing of the ST strip for long times (> 1000 h) at 800° C, however, causes hardening due to the formation of a precipitate, first at the grain boundaries (after a few hours of ageing) and then within the grains. The precipitate density increases with ageing time, reaching ~ 15 vol% (or more)

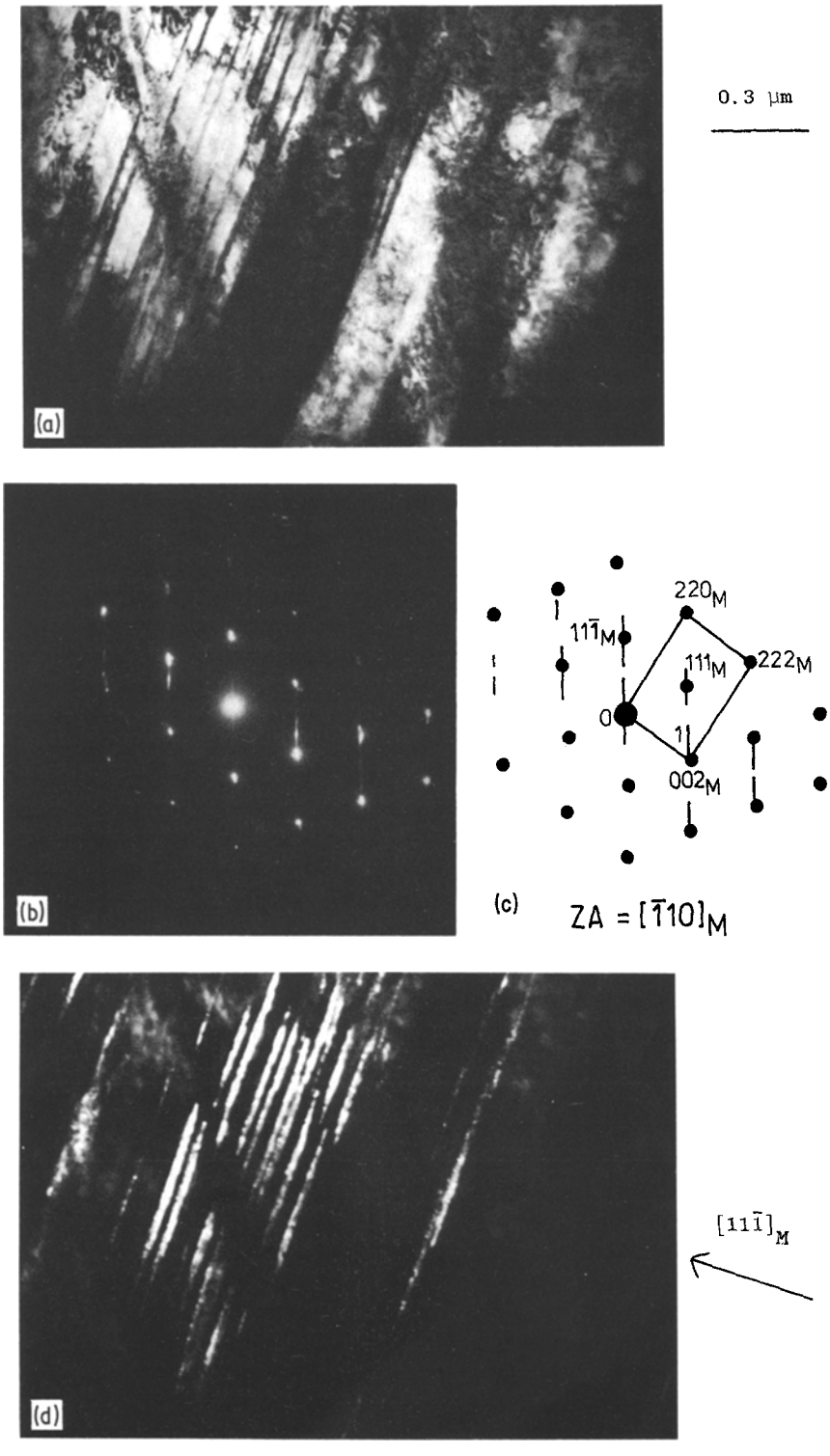

Figure 14 36% CW strip, aged 5 h at 500°C: (a) bright field; (b) SAD pattern of (a), with a $(\bar{1}\,1\,0)_M$ matrix orientation; (c) key to (b). • Common to all three phases; – streak or "relrod"; ZA = $[\bar{1}\,1\,0]_M$. (d) HRDF, from streak 1, showing thin platelets on $\{1\,1\,1\}$ planes.

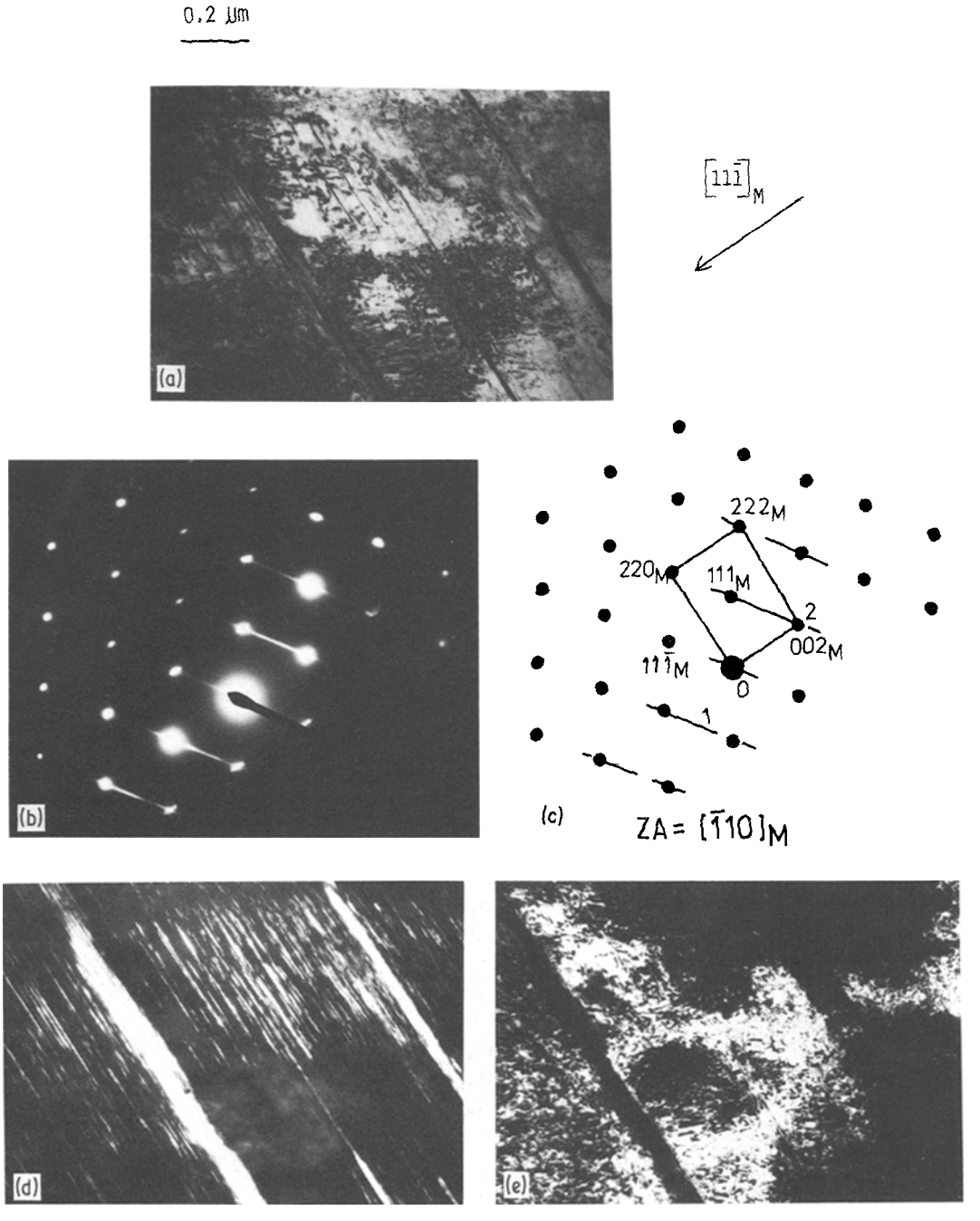

Figure 15 72% CW strip, aged 5 h at 500° C (peak hardness): (a) bright field; (b) SAD pattern of (a), with a $(1\,1\,0)_M$ matrix orientation; (c) key to (b). • Common to all three phases; – streak or "relrod"; ZA = $[\bar{1}\,1\,0]_M$. (d) HRDF, from streak 1, showing thin platelets on {1 1 1} planes; (e) HRDF, using spot 2 (i.e. $0\,0\,2_M$), which is common to all three phases.

after 1814 h at 800° C. The approximate composition of this intermetallic precipitate which also forms after long time ageing in the cold-worked samples (but without an overall hardening) is, in wt%, 45% Mo, 30% Co, 13% Cr, 5% Ni, 6% Fe, 1% Mn.

Age-hardening of Elgiloy at temperatures greater than 700° C, has not been reported previously in the literature. Henmi *et al.* [3], however, referred to the presence of some black spots in the bright field TEM micrographs of a 50% cold-rolled Elgiloy after ageing for 5 h at

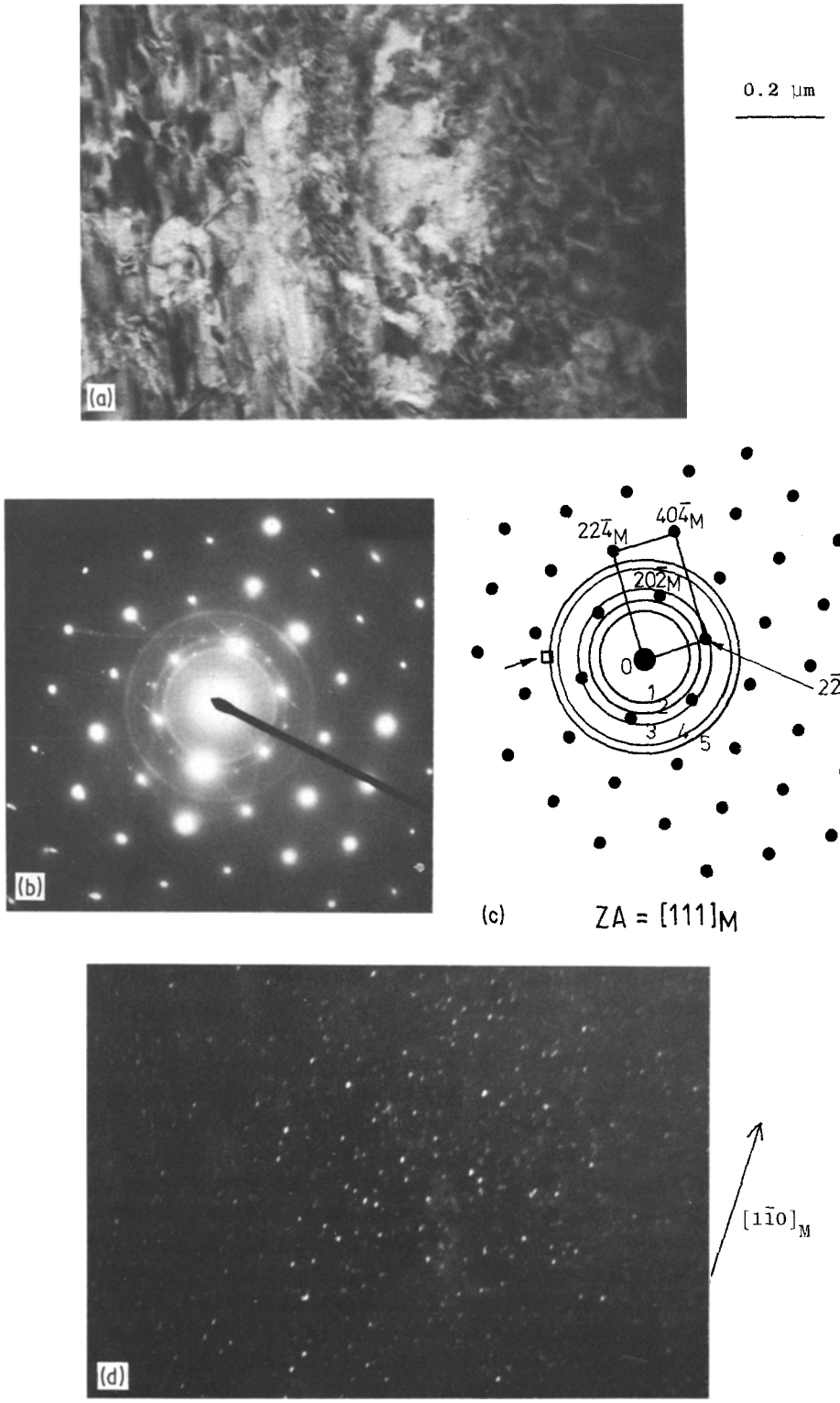

Figure 16 72% CW strip, aged 5 h at 500° C (peak hardness): (a) bright field; (b) SAD pattern of (a), with a $(1\,1\,1)_M$ matrix orientation. Note diffraction rings; (c) key to (b). • Common to all three phases; (Rings 1 to 5; ZA = $[1\,1\,1]_M$. (d) HRDF, from part of diffraction ring 5 (marked → □ in (c)), showing "fine" metallic oxide particles (surface contamination; see Table III).

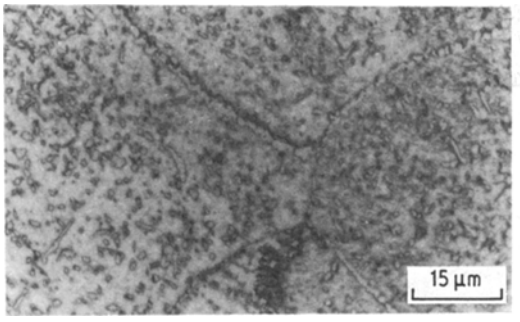

Figure 17 Optical micrograph of ST aged 1814 h at 800° C, showing precipitates at grain boundaries and within the grains.

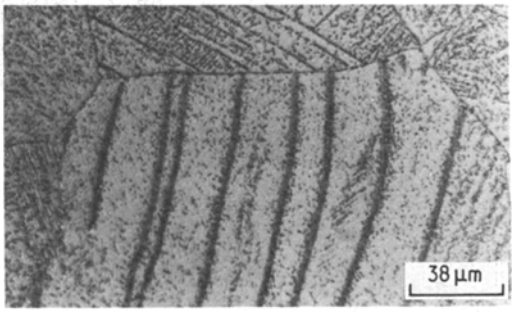

Figure 19 Optical micrograph of 36% CW, aged 1814 h at 800° C.

700° C, during which recrystallization of the matrix grains occurred, which were considered as either σ-phase (Co, Cr, Ni, Fe, Mn, Mo) or chromium carbides. Intermetallic compounds of σ, μ, π, laves and χ type have also been reported to form in a number of complex cobalt-based alloys after exposure to temperatures in excess of ~ 700° C [7, 27–29].

Lux and Bollmann [8] reported the precipitation of an intermetallic in the Co–Cr–Mo ternary system, the X-ray diffraction pattern of which was found to be almost identical to that of Co_7Mo_6 (μ-phase), of stoichiometric composition 58.25 wt% Mo–41.75 wt% Co. The chemical analysis of the extracted residues, however, indicated the presence of chromium in the precipitate, and it was suggested that molybdenum was partially replaced by chromium in the Co_7Mo_6 phase. The composition of the precipitate was 48% Mo, 39.6% Co, 12.5% Cr and its corresponding formula was given as $Co_7Mo_{5.2}Cr_{2.5}$. The extra peaks detected in the X-ray diffraction pattern of the ST Elgiloy aged 1814 h at 800° C closely matched some of the peaks reported by Lux and Bollmann [8]. As the main constitutents of this precipitate are molybdenum and cobalt and the d-spacings appear to be close to those of Co_7Mo_6, the basic structure is probably based on this compound, with chromium partially replacing molybdenum, and nickel and iron substituting partially for cobalt, to form a complex intermetallic compound.

In addition to the intermetallic phase, $M_{23}C_6$ carbides (M = Cr, Mo) were also detected in the ST samples after ageing at 800° C, and are also considered to contribute to the hardening observed at this temperature. $M_{23}C_6$ and other carbides have been observed in a number of cobalt-based alloys [28–32] after heat treatments at elevated

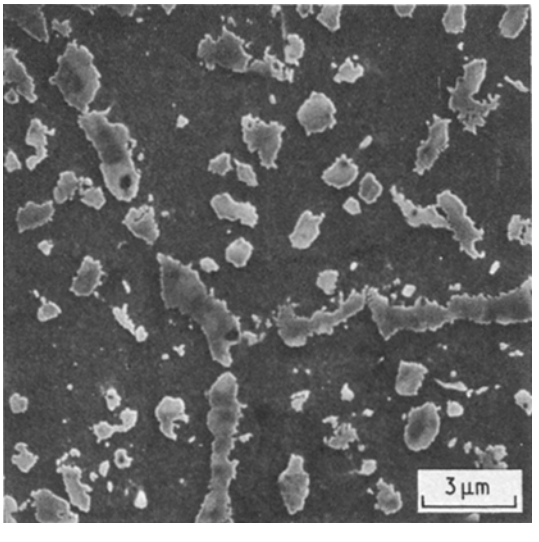

Figure 18 SEM micrograph of ST, aged 1814 h at 800° C, showing the precipitated phase at grain boundaries and within the grains.

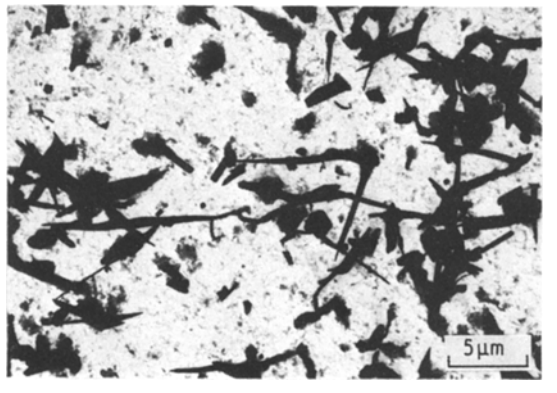

Figure 20 Bright field TEM micrograph of precipitates extracted from ST, aged 1814 h at 800° C strip.

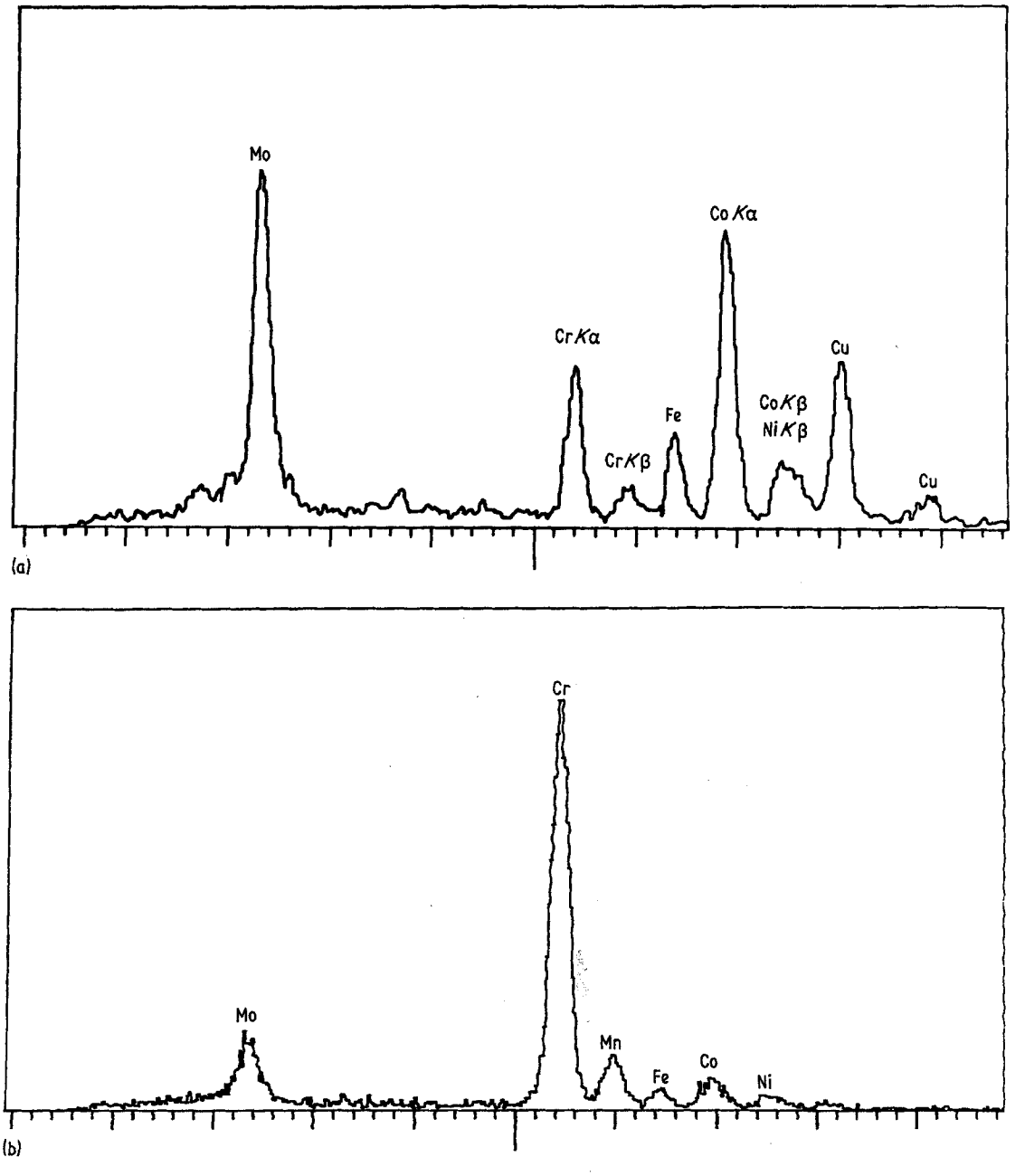

Figure 21 TEMSCAN, EDS analysis carried out on extracted precipitates of ST, aged 1814 h at 800° C strip. (a) Type 1 (majority) precipitates; (b) Type 2 (minority) precipitates.

temperatures. The low carbon content of Elgiloy (0.05 to 0.1 wt %) favours the formation of $M_{23}C_6$ in preference to M_7C_3. The crystal structure of $M_{23}C_6$ carbide is f c c, with a lattice parameter $a \simeq 1.08$ nm, which is higher than that reported for $Cr_{23}C_6$ ($a = 1.064$ nm). This expansion of the unit cell is perhaps due to the presence of molybdenum in the carbide which corresponds to a similar observation made in some Ni–Cr–Co–Mo alloys by Bollenrath and Rohde [7].

5. Conclusions

1. The solution treated (ST) or annealed Elgiloy consisted of a single phase solid solution with a f c c austenitic type crystal structure.

2. Cold-rolling of this f c c structure by 36%

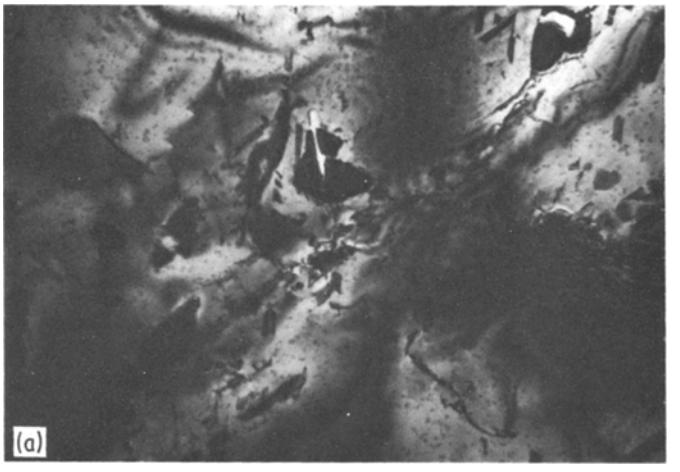

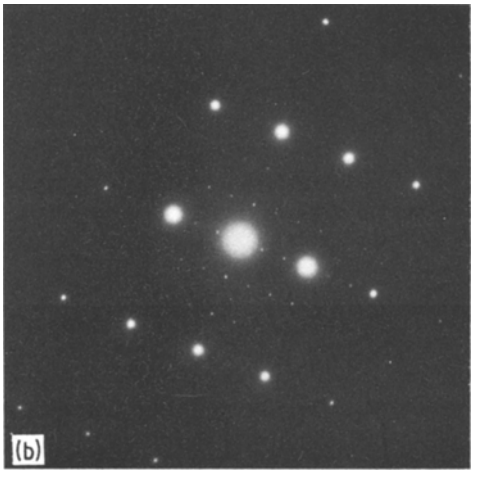

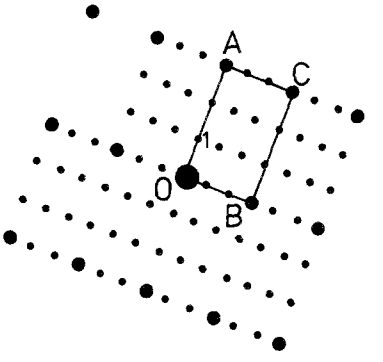

(c) $ZA = [112]_M$

Figure 22 ST, aged 1263 h at 800° C foil (a) bright field; (b) SAD pattern of (a); (c) key to (b): A = $(\bar{2}\,2\,0)_M = (\bar{6}\,6\,0)_P$, B = $(1\,1\,\bar{1})_M = (3\,3\,\bar{3})_P$, C = $(\bar{1}\,3\,\bar{1})_M = (\bar{3}\,9\,\bar{3})_P$, ZA = $[1\,1\,2]_M$; (d) HRDF using $(\bar{2}\,2\,0)_P$ precipitate reflection (spot 1).

and 72% at room temperature (36% CW and 72% CW strip) led to the formation of a network of thin lamellae of f c c deformation twins and h c p ϵ-platelets, the density of which increased with increasing cold-work. This was accompanied by a substantial strengthening of the alloy, attributed to the platelet networks.

3. Subsequent ageing of the cold-worked strip at 500° C caused further strengthening of the alloy. The ST condition, however, did not age-harden significantly at this temperature. The age-hardening of the cold-worked samples at 500° C was attributed to the formation of h c p ϵ-phase (via the $\alpha \rightarrow \epsilon$ transformation).

4. Ageing of the ST strip for long periods (> 1000 h) at 800° C caused an increase in hardness. This was accompanied by formation of a coarse Mo–Co–Cr intermetallic compound and $M_{23}C_6$ carbide. Ageing the cold-worked strips at 800° C caused a decrease in hardness which was attributed to the dissolution of the h c p ϵ-platelets and a reduction in dislocation density.

Acknowledgements

The authors gratefully acknowledge the provision of a University of London Studentship for M. Assefpour-Dezfuly together with the helpful support of Mr C. R. Milne, Radio and Navigation Division, Royal Aircraft Establishment in the supply of Elgiloy specimens.

References

1. R. E. TRICKEY, *J. Inst. Met.* 75 (1948/49) 890.
2. "Elgiloy", Alloy Digest (Aug. 1953) (published by Engineering Alloy Digest Inc., New Jersey).
3. Z. HENMI, M. OKADA and T. NAGAI, *Nippon Kinzoku Gakkai-Shi* **31** (1967) 1351.
4. P. LEGENDRE and Z. WACHE, International Conference on Chronometry, Vol. 2, 1964, p. 961.
5. H. J. KESTENBACH, *Metallography* **10** (1977) 189.
6. D. W. PASHLEY and M. J. STOWELL, *Phil. Mag.* 8 (1963) 1605.
7. F. BOLLENRATH and W. ROHDE, *Cobalt* **34** (1967) 18.
8. B. LUX and W. BOLLMANN, *ibid.* **11** (1961) 4.
9. J. M. DRAPIER, P. VIATOUR, D. COUTSOURADIS and L. HABRAKEN, *ibid.* **49** (1970) 171.
10. A. H. GRAHAM, *Trans. ASM* **62** (1969) 930.
11. A. H. GRAHAM and J. L. YOUNGBLOOD Met. Trans. 1 (1970) 423.
12. M. RAGHAVAN, B. J. BERKOWITZ and R. D. KANE, *ibid.* **11A** (1980) 203.
13. G. GONZALEZ DE ARMENGOL, PhD thesis, University of London (1981).
14. L. REMY and A. PINEAU, *Met. Trans.* **5** (1974) 963.
15. L. MANGONON Jr and G. THOMAS, *ibid.* **1** (1970) 1577.
16. M. W. BOWKETT and D. R. HARRIES, AERE report, R-9093 (1978).
17. H. J. KESTENBACH, *Met. Assoc. Brazileira Met.* **32** (1976) 181.
18. H. T. MICHELS and R. M. FORBES-JONES, *Met. Trans.* **5** (1974) 847.
19. L. REMY and A. PINEAU, *Mater. Sci. Eng.* **26** (1976) 123.
20. T. ERICSSON, *Acta Metall.* **14** (1966) 853.
21. E. H. KOSTER, A. R. THOLEN and A. HOWIE, *Phil. Mag.* **10** (1964) 1093.
22. T. C. TISONE, *Acta Metall.* **21** (1973) 229.
23. W. BONFIELD and B. C. EDWARDS, *J. Mater. Sci.* 9 (1974) 398.
24. *Idem, ibid.* 9 (1974) 409.
25. *Idem, ibid.* 9 (1974) 415.
26. I. PFEIFFER, *Z. Metallkunde* 57 (1966) 635.
27. Cobalt Monograph, Centre D'Information Du Cobalt, Brussels, (1960).
28. J. W. WEETON and R. A. SIGNORELLI, NACA Technical Note 3109 (1954).
29. C. P. SULLIVAN, M. J. DONACHIE Jr and F. R. MORRAL, Cobalt-base superalloys, Centre D'Information Du Cobalt, Brussels (1970).
30. B. LUX and W. BOLLMANN, *Cobalt* **12** (1961) 32.
31. V. RAMASWAMY, P. R. SWANN and D. R. F. WEST, Proceedings of the Fifth International Materials Symposium Berkeley, California, 1972, p. 637.
32. P. A. BEAVEN, P. R. SWANN and D. R. F. WEST, *J. Mater. Sci.* **14** (1979) 354.

Received 7 October
and accepted 1 November 1983